Bifunctional Intimacy and its Interplay with Metal-Acid Balance in Shaped Hydroisomerization Catalysts

Pedro Mendes, João Silva, M. Filipa Ribeiro, Antoine Daudin, Christophe Bouchy

Bifunctional intimacy and its interplay with metal-acid balance in shaped hydroisomerization catalysts

Pedro S. F. Mendes[a,b,1*], João M. Silva[a,c], M. Filipa Ribeiro[a], Antoine Daudin[b], Christophe Bouchy[b*]

[a]*Centro de Química Estrutural and Departamento de Engenharia Química, Instituto Superior Técnico, Universidade de Lisboa, Av. Rovisco Pais, 1049-001 Lisboa, Portugal*

[b]*IFP Energies nouvelles, Rond-point de l'échangeur de Solaize, BP 3, 69360 Solaize, France*

[c]*ADEQ-ISEL, Instituto Superior de Engenharia de Lisboa, Instituto Politécnico de Lisboa, R. Cons. Emídio Navarro, 1959-007 Lisboa, Portugal*

*pedro.mendes@tecnico.ulisboa.pt; christophe.bouchy@ifpen.fr ; +33 (0)4 37 70 28 60

This is the submitted, **non-peer reviewed** version of the following article: P. S. F. Mendes, J. M. Silva, M. F. Ribeiro, A. Daudin, C. Bouchy, *ChemCatChem* **2020**, *12*, 4582–4592, which has been published in final form at https://doi.org/10.1002/cctc.202000624.

[1] Present address: Laboratory for Chemical Technology, Ghent University, B-9052 Ghent, Belgium

Abstract

The combined impact of platinum location and metal-acid balance on the catalytic performances of HUSY zeolite alumina-shaped bifunctional catalysts was evaluated in the *n*-hexadecane hydroisomerization. For well-balanced catalysts, the location of Pt on the alumina resulted in lower isomerization selectivity as compared to when platinum was located on the zeolite. In the latter case, the maximal distance between Pt and acid sites was found to be in the nanometric scale (high intimacy) whereas in the former it was in the micrometric scale (low intimacy), particularly due to the presence of large clusters of HUSY zeolite. Nevertheless, whenever proper balance between functions was not ensured in high-intimacy catalysts, the low-intimacy were shown to perform better. The requirement for nanometric metal-acid sites intimacy must be hence combined with an adequate metal-acid balance to achieve optimal catalytic performance.

Introduction

Bifunctional catalysts comprising acid and hydrogenation-dehydrogenation functions are at the heart of the petroleum refining industry (e.g. hydroisomerization of C_5-C_6 [1], hydrocracking of heavy oil cuts [1-2], dewaxing by hydroisomerization [3]). Due to their flexibility towards different products [2, 4] and the number of solutions available to tackle different catalyst poisons [2], bifunctional catalysts will also play a key role in the production of sustainable fuels from a panoply of feedstocks (e.g. vegetable oils [5], Fischer-Tropsch waxes [6], (pyrolyzed) plastic waste [7]).

The hydroisomerization of long chain *n*-paraffins involves such a bifunctional catalyst typically consisting of a noble metal finely dispersed over a support in which a zeolite is shaped with a binder in the form of extrudates. Designing a bifunctional catalyst is thus a complex process where numerous parameters might play a role. In order to reduce the degree of complexity, most studies have been carried out over unshaped zeolite catalysts in the powder form. The focus is then frequently put on the study of the effect of zeolite properties on the hydroisomerization performance. Particularly, by varying the pore architecture and acid-base properties [8]. The observed effects shall, nevertheless, be taken cautiously, as those originate from powder zeolite catalysts whereas shaping with a binder, typically alumina or silica, is required for the industrial applications [9]. Shaping is commonly described as a complex process that might significantly modify the active sites of the zeolite [10], which is far from being fully understood [11]. The few available studies report either neutralization of the most acidic Brønsted sites [12] or, conversely, increased acidity upon shaping of zeolite [13]. However, full preservation of zeolite properties has been also achieved [14], resulting in similar catalytic behaviour for hydroconversion reactions prior to and after shaping [14a].

According to the classical bifunctional mechanism [15], optimal catalytic performance is achieved when the acid function is “well-balanced” by the hydrogenating-dehydrogenating (HDH) function [8b, 16]. In such case, for fixed operating conditions, the catalytic performance in hydroisomerization is solely dictated by the zeolite properties. Kinetically, this implies that the rate-determining reaction steps take place in the zeolite. The HDH function must be hence sufficiently active as compared to the acid function[8b, 15, 17]. Moreover, to prevent undesirable consecutive reactions over acid sites, the distance between these functions (Weisz’s intimacy criterion) must also be sufficiently short [18]. Therefore, both the ratio and the distance between metal and acid sites must be controlled when designing industrial bifunctional catalysts.

In the particular case of the metal-acid sites distance (or, inversely, intimacy), most of the studies have shown that sufficient proximity between metal and acid sites enhances the selectivity towards feed isomers [18-19]. Recent reports have, however, reopened the debate about the ideal proximity between both functions for optimal performances [20]. In the most noteworthy case, improved yield in feed isomers was observed when the platinum was deposed on the alumina and not on the zeolite [20a]. Nevertheless, the effect of the metal to acid sites ratio was not

evaluated. Additionally, shaping introduces additional complexity, as the dimensions of the extrudate may introduce mass transfer limitations [21]. In order to assess the intrinsic catalyst properties the size of the extrudate will then likely need to be reduced, which can alter the catalytic properties of the tested sample as compared to the extrudate properties whenever Pt is heterogeneously distributed in the extrudate [14a].

In this study, the sole effect of metal location on the catalytic properties of industrially-relevant hydroisomerization catalysts was firstly investigated, by carefully controlling all the other parameters. To probe the catalytic behaviour of shaped zeolite catalysts featuring platinum nanopartices either on the binder or on the zeolite, *n*-hexadecane hydroisomerization was chosen. To isolate the effect of the metal location, the metal to acid sites ratio was also varied enabling the evaluation of catalysts with fixed (optimal) metal to acid sites ratio and distinct metal location. Taking that knowledge, the combined role of metal-acid intimacy and balance was then assessed. Any significant temperature effect was prevented by mainly varying the reactant conversion thanks to the hydrocarbon space time, keeping a narrow range of temperatures. Further experimental artefacts like mass and heat transfer limitations were excluded by careful design of the experimental tests. Finally, the catalysts were compared via metrics intrinsic to their catalytic behaviour in hydroisomerization: the turnover frequency over the Brønsted acid sites and the maximum feed isomers yield.

Results

Catalysts characterization

Zeolite and support

The physico-chemical properties of the HUSY zeolite and the corresponding alumina-shaped extrudates will be briefly described, as both solids have been previously characterized in detail in [22] and [14a], respectively. FAU topology has a 3-dimensional channel with an equivalent minimum pore size of 0.74 nm, giving rise to 1.4 nm supercages at the channel intersections [23]. This leads to a large micropore volume and surface area, as observed in the commercial sample employed herein (Table 1). The framework Si/Al atomic ratio amounted to 18.4, resulting in a concentration of framework aluminium Al^{IV} of 820 µmol g^{-1} [24](Table 1). As these aluminium atoms generate negatively charged oxygen atoms in zeolites framework [23], their concentration provides a good estimation of Brønsted acid sites concentration for zeolites in the protonic form.

Table 1: Zeolite fractions, Al^{IV} concentrations, micro and mesopores properties by N_2 adsorption-desorption [14a].

Sample	Si[a] (wt.%)	Zeolite (wt.%)	$n_{Al(IV)}$ (µmol g^{-1})	V_{micro} (mL g^{-1})	S_{micro} (m^2 g^{-1})	V_{meso} (mL g^{-1})	S_{meso} (m^2 g^{-1})
HUSY	43.9	100	820	0.33	813	0.21	101
Al_2O_3+HUSY	7.3	16.5[b]	135[c]	0.045	105	0.59	266

[a] Measured by X-ray fluorescence.
[b] Using the amount of Si measured by X-ray fluorescence in parent zeolite.
[c] Using $n_{Al(IV)}$ determined for the parent zeolite.

According to the weight percentage of silicon, the trilobe extrudates comprised roughly 83.5 wt % of alumina and 16.5 wt % of HUSY zeolite (Table 1). The characterization of the extrudates after calcination only revealed γ-Al_2O_3 and FAU framework phases, with no evidence of crystallinity loss upon shaping [14a]. The microporous volume of the shaped supports corresponded to more than 80% of that of the parent zeolite. The same activity per zeolite mass for shaped and unshaped USY was obtained in a model reaction catalysed by Brønsted acid sites (m-xylene conversion) [14a]. Hence, all the evidences pointed towards a full preservation of the zeolite properties in the shaped Al_2O_3+HUSY sample. The concentration of Brønsted acid sites in the extrudate was, hence, directly estimated based on that of parent zeolite (Table 1).

Metal

The metal properties of the samples are presented on Table 2. For both catalyst series, the actual Pt loadings were lower than the nominal ones, which can be attributed to a fractional ionic exchange efficiency [14a]. The accessible metal on the samples was determined by oxygen titration of chemisorbed hydrogen. The corresponding metal dispersions were quite high, with Pt being better dispersed in alumina (ca. 90 %) as compared to in HUSY (ca. 73%). The very low Pt content

in 0.04Pt/Al_2O_3+HUSY precluded the evaluation of Pt dispersion by O_2-H_2 titration. The average value of dispersion for the other Pt/Al_2O_3+HUSY samples was then used to estimate the concentration of accessible metal sites in that sample. Assuming that the concentration of Brønsted acid sites in the catalysts was similar to that of the shaped support, the metal to acid sites molar ratio (n_{Pt}/n_{Al}) was estimated for each catalyst. The variation in platinum loadings resulted in clear distinct n_{Pt}/n_{Al} within each catalyst series. Furthermore, both catalyst series had a similar n_{Pt}/n_{Al} range, as aimed at for a meaningful comparison of the catalysts performances in *n*-hexadecane hydroconversion.

Table 2: Pt loading and dispersion, accessible Pt and metal to acid sites molar ratio for bifunctional catalysts.

Catalyst	Nominal Pt loading (wt.%)	Measured Pt loading (wt.%)	Dispersion (%)	n_{Pt} [b] (μmol g^{-1})	n_{Pt}/n_{Al}	Pt distribution coefficient
0.11Pt/HUSY+Al_2O_3	0.125	0.11	71	4	0.030	0.95
0.25Pt/HUSY+Al_2O_3	0.375	0.25	76	10	0.071	0.99
0.04Pt/Al_2O_3+HUSY	0.050	0.04	<MDL	2[a]	0.015	1.00
0.07Pt/Al_2O_3+HUSY	0.080	0.07	91	3	0.024	0.95
0.18Pt/Al_2O_3+HUSY	0.200	0.18	89	8	0.061	0.95

[a] Assuming a Pt dispersion of 90% (average of other Pt/Al_2O_3+HUSY samples).
[b] Accessible Pt as measured by O_2-H_2 titration.

To have a quantitative overall picture of the Pt location, the distribution of chemical elements along the diameter of extrudates was measured by Electron Probe Micro Analysis (EPMA). Figure 1 depicts the average elemental profiles of Al, Si, and Pt for 0.25Pt/HUSY+Al_2O_3 and 0.18Pt/Al_2O_3+HUSY samples, as an example (all profiles can be found in SI). The platinum concentration profiles revealed a uniform distribution of platinum along the diameter of the extrudates for both samples. This was further investigated by calculating the distribution coefficient for platinum (vide Experimental Section). All samples featured a distribution coefficient above 0.95 (Table 2), confirming the uniform distribution of platinum along the extrudates. Nonetheless, it is worth mentioning that small variations in the metal loading (particularly, towards lower values) or synthesis procedures can lead to non-uniform metal distributions [14a].

The concentration profiles of Al and Si (Figure 1) also show quite a uniform distribution along the extrudates, pointing out to a uniform distribution of zeolite in the alumina matrix, as previously observed as well for this support [14a]. The minor variations observed were similar but in opposite directions: whenever Si concentration increased, that of alumina decreased and vice-versa. This enabled the identification of zeolite-rich (in presence of silicon) and alumina-rich (in absence of silicon) domains along the extrudates. The Pt content in either the zeolite or the alumina, depending on the catalyst series, was thus estimated (vide Experimental Section for calculations details) and compared to the Pt content deposed in the whole support (Figure 2).

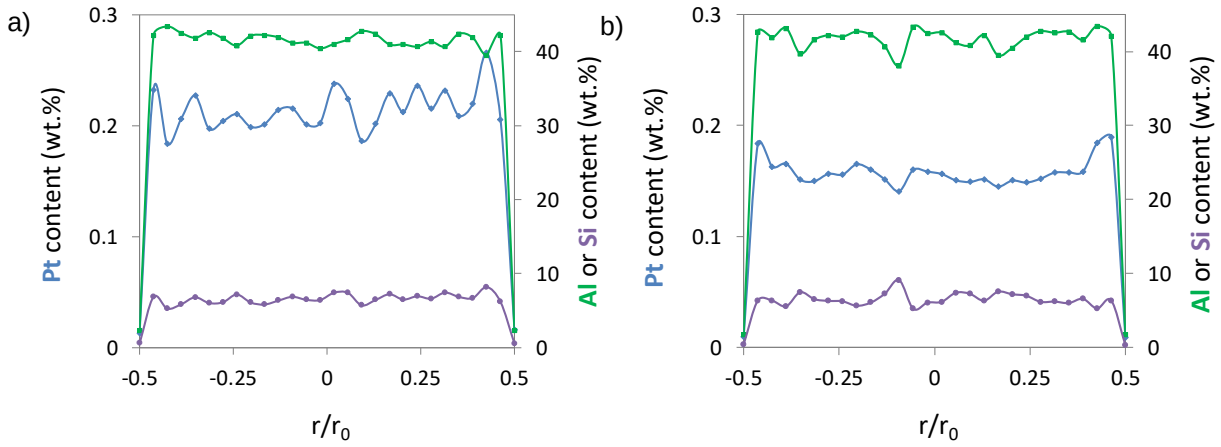

Figure 1: Average electron probe microanalysis profiles of Pt (blue), Al (green), and Si (purple) along the diameter of the extrudate for a) 0.25Pt/HUSY+Al_2O_3 [14a] and b) 0.18Pt/Al_2O_3 +HUSY.

For Pt/HUSY+Al_2O_3 samples, the Pt content deposed in the HUSY zeolite nearly matched the overall Pt deposed in the support (Figure 2), as previously disclosed [14a]. Conversely, for Pt/Al_2O_3+HUSY, the Pt content deposed in the alumina matched the overall Pt deposed in the support (Figure 2). A selective deposition of platinum on either the zeolite or the alumina was, hence, achieved via well-suited metal deposition methods. More specifically, the methods employed take advantage of the different acid-base properties of the alumina and the HUSY zeolite in solution. The point of zero charge of γ-Al_2O_3 is usually attained at a pH around 7-8 [25], whereas for HUSY zeolite the charge neutrality in solution was measured at a pH of 3. Therefore, in weak acidic medium the surface of alumina should be positively charged, contrarily to that of the zeolites. The $PtCl_6^{2-}$ anions are thus preferably deposed on the alumina while the $Pt(NH_3)_4^{2+}$ cations are preferably deposed on the HUSY zeolite [20a, 24].

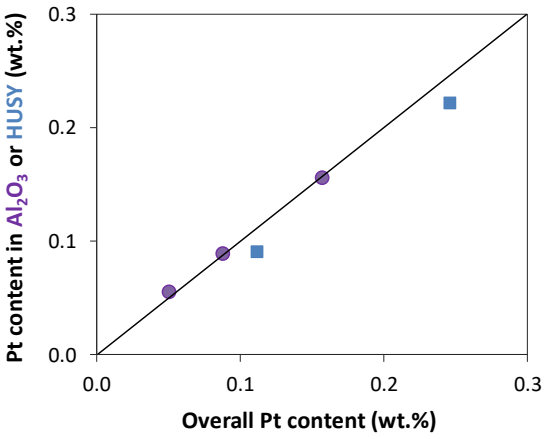

Figure 2: Pt content deposed on the HUSY zeolite for Pt/HUSY+Al_2O_3 (■) samples [14a] and deposed on the support for Pt/Al_2O_3+HUSY (●) catalyst series vs. overall Pt content.

Hydroisomerization of *n*-hexadecane

Turnover frequency over Brønsted acid sites

The turnover frequency was chosen to evaluate the intrinsic activity of the Brønsted acid sites in the bifunctional catalysts. Whenever the limiting reactant conversion is significant, the rate law must be known to compute the average turnover frequency along the reactor. In the case of *n*-paraffins hydroconversion, it has been repeatedly confirmed that the overall reaction follows a first-order kinetics in the paraffin concentration [8b, 25]. In Figure 3, first-order plots are showcased for 0.18Pt/Al_2O_3+HUSY catalyst (vide SI for other catalysts). Irrespectively of reaction temperature, the quality of the fitting was high confirming once again the previous observations. Making use of the first-order kinetic constant, the average turnover frequency per protonic sites (TOF_{Al}) was determined for all catalysts at every temperature. The apparent activation energy was in the 180-196 kJ mol^{-1} range. Acknowledging the possible influence of metal to acid sites ratio [8b, 16a], TOF_{Al} of the catalyst series were compared as a function of n_{Pt}/n_{Al} at 488 K in Figure 3b).

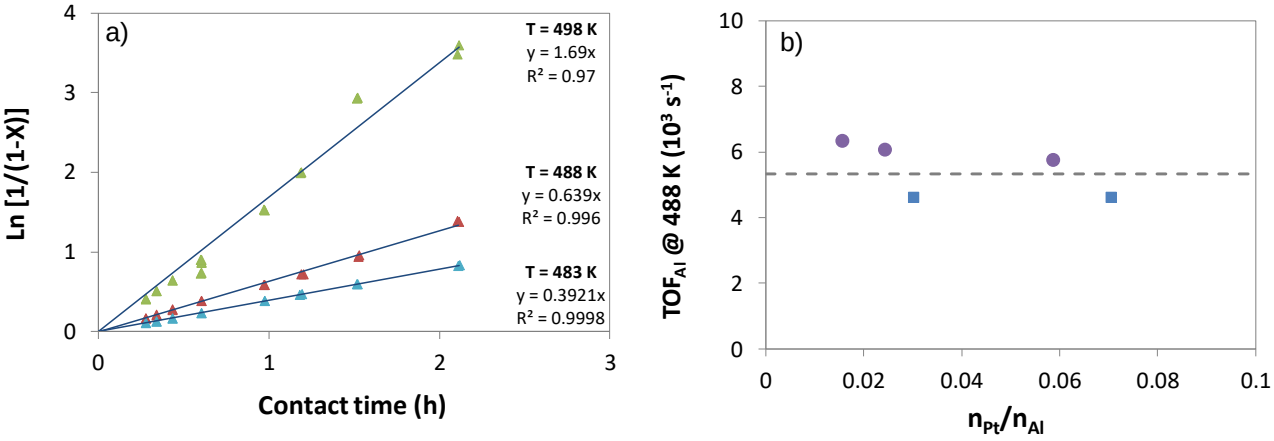

Figure 3: a) First-order plot for the consumption of *n*-hexadecane at 1.1 MPa total pressure and a molar H_2 to *n*-C_{16} ratio of 10 over 0.18Pt/Al_2O_3+HUSY catalyst. Symbols stand for experimental data and lines for fitting results. b) Turnover frequency per protonic site as a function of n_{Pt}/n_{Al} ratio. Pt/HUSY+Al_2O_3 [14a] (■) and Pt/Al_2O_3+HUSY (●) catalyst series. Dashed line corresponds to the average turnover frequency.

In spite of the significant variation in the metal to acid sites ratio (ca. 4 times), the turnover frequency remained constant over both catalyst series. The insensitivity of TOF_{Al} to metal-acid site ratio has been reported in several studies, being a direct consequence of the reaction mechanism for relatively high n_{Pt}/n_{Al} [8b, 16a]. Qualitatively, variations on the amount of HDH function will not impact the turnover frequency, because the dehydrogenation rate is anyway sufficient to feed all the Brønsted sites with intermediate olefinic species [16a]. In other words, the dehydrogenation of *n*-hexadecane is considerably faster than the conversion of its olefinic intermediate over the acid sites, the acid-catalysed conversion remaining, hence, the rate-limiting step regardless of n_{Pt}/n_{Al}. More importantly, the TOF_{Al} value obtained over both catalysts series

was comparable. The minor difference might indicate a slight loss of acidity upon Pt deposition on the zeolite. In any case, these results revealed that the Brønsted acid sites held a similar intrinsic activity regardless of location of the HDH function (on the alumina or on the zeolite).

Yield in C_{16} isomers

The hydroisomerization selectivity of the catalysts was evaluated via the evolution of the yield in isomerization products of *n*-hexadecane as function of conversion (Figure 4). For Pt/HUSY+Al_2O_3 catalysts (Figure 4a), the evolution of C_{16} isomers yield with conversion was analogous. Nonetheless, a slight increase in the maximal C_{16} isomers yield (i.e. at ca. 80% conversion) was observed when increasing the Pt loading from 0.11 to 0.25%. The results disclosed for the Pt/Al_2O_3+HUSY series (Figure 4b) were somewhat similar. Despite the similar evolution of the yield curves, a clear increase of the maximal C_{16} isomers yield with the Pt loading could be recognized. For the sake of completeness, the effect of temperature on the feed isomer yield was assessed and confirmed to be negligible in the narrow range of temperatures chosen (vide SI).

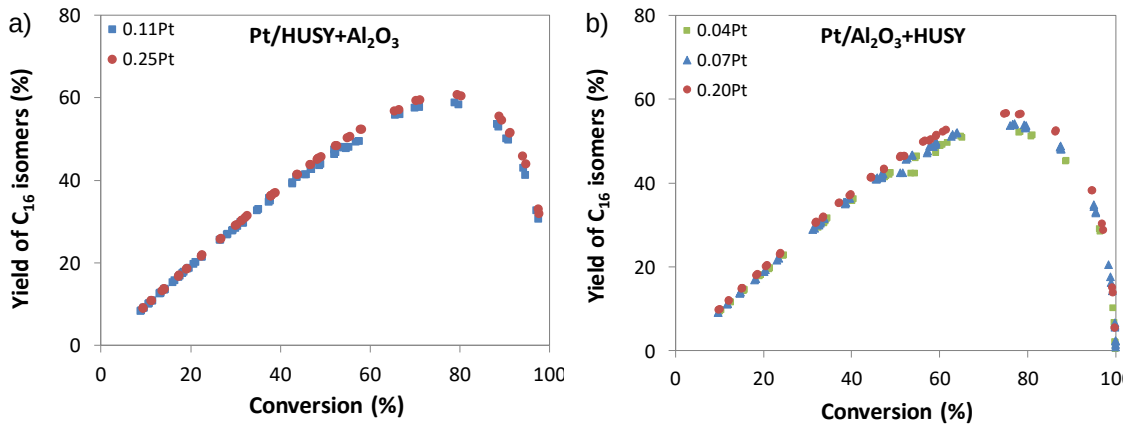

Figure 4: Yield of feed isomers as function of conversion over a) Pt/HUSY+Al_2O_3 series [14a] and b) Pt/Al_2O_3+HUSY catalyst series.

To further evaluate the influence of the metal to acid sites ratio, the dual-function kinetic model, previously proposed by us [8b] and validated over different catalytic systems [8b, 26] and hydroconversion reactions [19a], was employed. This model based on lumped products establishes a unique relation between the maximal C_{16} isomers yield ($Y_{i\text{-}C16}$) and the metal to acid sites molar ratio, for a given zeolite tested at similar operating conditions (Eq. 3).

$$Y_{i-C_{16}} = \frac{\gamma}{1 + \varepsilon(n_{Al}/n_{Pt})} \qquad \text{Equation 3}$$

The estimated values for the parameters ε and γ can be found in Supporting Information. The comparison of catalysts series is presented in Figure 5 through the evolution of maximal C_{16} isomers yield ($Y_{i\text{-}C16}$) with n_{Pt}/n_{Al}. The metal to acid sites ratio had a rather similar effect on the maximal C_{16} isomers yield over both catalyst series. Specifically, the plateaux of $Y_{i\text{-}C16,max}$ were

seemingly achieved at the same level of n_{Pt}/n_{Al}. This plateau behaviour of the maximal C_{16} isomers yield can be explained at the light of the bifunctional mechanism by fast rates of hydrogenation/dehydrogenation compared to the acid-catalysed isomerization and cracking ones [15]. The latter being the rate-determining steps, the apparent reaction scheme is thus governed by the zeolite properties and thereby intrinsic to the zeolite [8b]. The bifunctional catalyst is, then, labelled "well-balanced" and its behaviour does not depend on the metal-acid sites ratio.

Strikingly, depending on the platinum location, the well-balanced shaped catalysts had markedly different $Y_{i\text{-}C16,max}$. At the maximum experimental n_{Pt}/n_{Al} (see Figure 4), the Pt/HUSY+Al_2O_3 series achieved a yield of 60.6 % whereas the Pt/Al_2O_3+HUSY series achieved a yield of 56.5 %. According to the dual-function kinetic model, at maximum $Y_{i\text{-}C16,max}$ attainable (i.e. at infinite n_{Pt}/n_{Al}) over the two series is 62.3 % and 58.3 %, respectively. Hence, despite both catalyst series have featured the same zeolite and appropriate metal to acid sites molar ratios, Pt/Al_2O_3+HUSY catalysts achieved lower maximal C_{16} isomers yield than Pt/HUSY+Al_2O_3. To further investigate this loss of feed isomers, we will now focus exclusively on the product selectivities over the well-balanced catalysts.

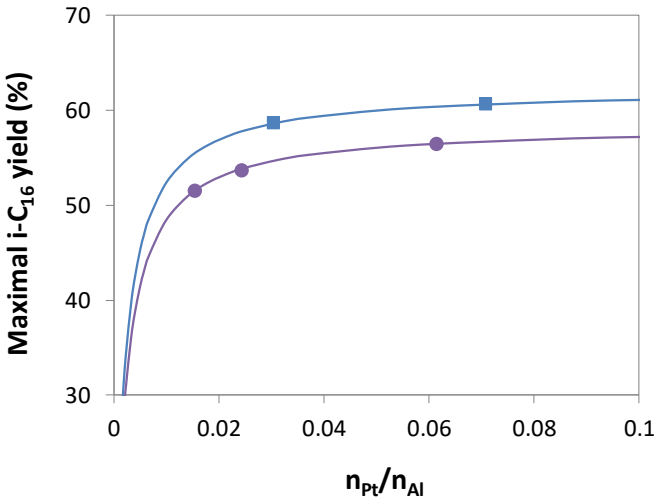

Figure 5: Maximal C_{16} isomers yield as a function of the overall n_{Pt}/n_{Al} molar ratio. Pt/HUSY+Al_2O_3 (■) [14a] and Pt/Al_2O_3+HUSY (●) catalyst series. Symbols stand for experimental data and lines for model fitting results.

Product distributions over well-balanced catalysts

Figure 6 depicts the product distribution in terms of lumps as a function of conversion for the well-balanced catalysts: 0.25Pt/HUSY+Al_2O_3 and 0.18Pt/Al_2O_3+HUSY. Focusing on the low conversion range and visually extrapolating to zero conversion, the selectivity towards both monobranched (MB) and multibranched (MTB) isomers of hexadecane seemed to be non-negligible. Both were, hence, primary products of the hydroconversion reaction. Nonetheless, the MB isomers clearly outweighed the MTB ones. MB products were predominant at conversion levels lower than 50 % whereas MTB products took over for conversions between 50 % and 90

%. The selectivity towards cracking products (CP) remained relatively insignificant up to 40 % of conversions, becoming increasingly important as conversion increased. Such exponential increase in selectivity with conversion is characteristic of products formed via a reaction intermediate (i.e. non-primary products) and not consumed by any further reaction. This is indeed the case for cracking products (CP) as all products were considered together into the same lump. Taking all the observations into account, one could infer that the hydroconversion reactions occurred in a rather consecutive manner: n-C_{16} → MB → MTB → CP.

Comparing the catalysts at low conversions, 0.25Pt/HUSY+Al_2O_3 presented a higher MB/MTB ratio than 0.18Pt/Al_2O_3+HUSY (Figure 6). At high conversions, selectivity towards both MB and MTB isomers was lower over the latter. As a result, cracking selectivity was more significant over 0.18Pt/Al_2O_3+HUSY. The apparent reaction scheme was somewhat more parallel when platinum was deposed on Al_2O_3 than when it was deposed on the zeolite HUSY itself. From the mechanistic point of view, that is typically associated with longer residence times of intermediate olefins, resulting in more consecutive acid-catalysed reactions and, thereby, a more parallel apparent reaction scheme [4, 8b, 16a]. However, this could not be attributed to metal-acid balance (as both catalysts were well-balanced) nor to the properties of the acid function as the support and the zeolite at stake were the same. On the other hand, Pt was located either on the zeolite (Pt/HUSY+Al_2O_3) or on the alumina (Pt/Al_2O_3+HUSY). Acknowledging the possible role of the distance between metal and acid sites [16b, 18a, 20a], a closer look will be taken at this parameter.

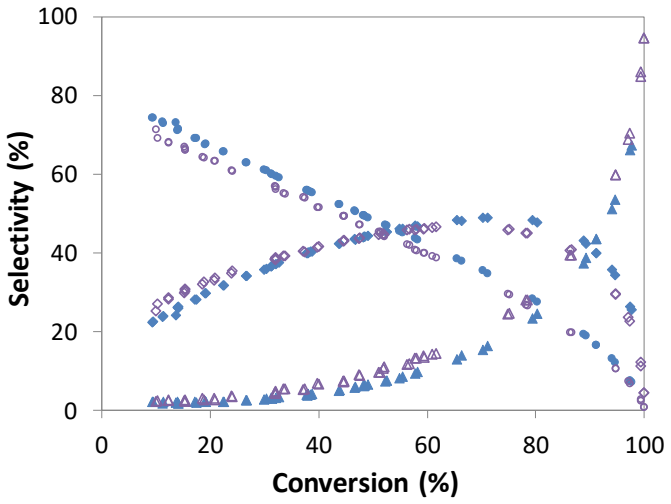

Figure 6: Monobranched (circles) and multibranched (diamonds) C_{16} isomers, and cracking products (triangles) selectivity as function of conversion over 0.25Pt/HUSY+Al_2O_3 (closed symbols) and 0.18Pt/ Al_2O_3+HUSY (open symbols).

Discussion

Estimation of the metal-acid sites distance

While the experimental determination of (a distribution of) the metal-acid sites distance would be a daunting task, the estimation of the maximal distance can be fairly straightforward if the Pt location is known. When platinum is homogeneously dispersed in the zeolite, the maximum distance between Pt and acid sites corresponds to half of the distance between two consecutive Pt particles [14a]. As Pt has been observed to be homogeneously distributed both inside the zeolite HUSY crystals [22b] and throughout the support on the employed Pt/HUSY+Al_2O_3 catalysts (Figure 1a), the calculations were grounded on such premise. For Pt/HUSY+Al_2O_3 catalysts, the maximum Pt-acid sites distance was revealed to be between 10 and 20 nm, depending on the Pt concentration in the zeolite crystals (Table 3). An analogous range was also obtained for Pt deposed on pure zeolite (Pt/HUSY).

Table 3: Maximal Pt-acid distance at the nanoscale.

Sample	Critical distance	Dependence on Pt loading	$d^{max}_{Pt\text{-}acid}$ (nm)
Pt/HUSY	Pt-Pt	Yes	**15-20**
Pt/HUSY+Al_2O	Pt-Pt	Yes	**10-20**
Pt/Al_2O_3+HUSY	Size of zeolite agglomerates	No	**100-10000**

In the case of Pt/Al_2O_3+HUSY samples, the results of EPMA have shown that the whole Pt is virtually located in the alumina. On the other hand, besides single crystals, also porous clusters of zeolite HUSY are present in the extrudates [14a]. Those can be as large as $2{\cdot}10^4$ nm size [14a]. Consequently, as sketched in Figure 7, the Pt-acid sites distance is abruptly maximized whenever zeolite clusters are at stake. In such case, the maximum distance is uniquely defined by the cluster size (Figure 7) being hence as long as 10 µm (half of the maximal clusters size).

Nevertheless, the clusters of zeolite corresponded only to a fraction of the whole zeolite present in the shaped Al_2O_3+HUSY support [14a]. Therefore, the case of single zeolite crystals should be also evaluated. According to Figure 7, for a single crystal of zeolite, the maximal Pt-acid sites distance corresponds to half of the sum of Pt-Pt distance to the crystal size. The Pt-acid distance was thus estimated considering a homogeneous Pt distribution and a bulk density for the alumina of 1.2 g cm^{-3}. From 0.04 to 0.18 wt.% of Pt loading, $d_{Pt\text{-}Pt}$ ranged from 35 to 20 nm. According to SEM measurements, the size of zeolite HUSY crystals in the shaped support ranges from 300 to 1000 nm [14a]. In that way, the maximal Pt-acid distance would be ca. 520 nm in Pt/Al_2O_3+ HUSY. Thereby, the Pt-acid sites distance would be more than 10 times larger in Pt/Al_2O_3+USY than in Pt/HUSY+Al_2O_3 extrudates.

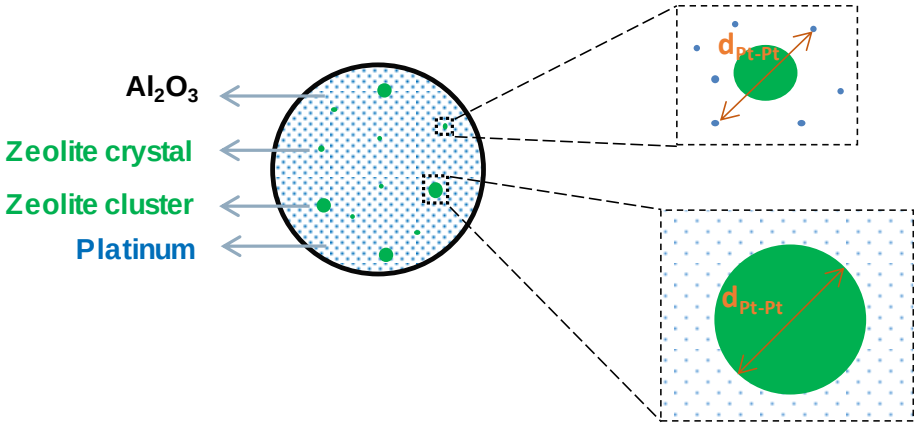

Figure 7: Schematic representation of a Pt/Al_2O_3+HUSY cross section focusing on the maximal Pt-acid sites distance in the case of single zeolite crystals (top magnification) and clusters of zeolites (bottom magnification). Actual extrudate diameter: 1.6 mm. Actual crystal size: $1 \cdot 10^3$ nm. Actual cluster size: $2 \cdot 10^4$ nm. Actual Pt nanoparticles size: 1.1 nm.

In summary, the presence of zeolite agglomerates can amplify up to 4000 times the Pt-acid site distance. The size of zeolite agglomerates is thus the critical size for Pt-acid sites distance when metal is located in the Al_2O_3. Nonetheless, the gap of several orders of magnitude between crystal and cluster sizes implies that the fraction of zeolite present in clusters may be of relevance to the actual implications of the metal to acid sites distance. Quantifying this fraction via routine techniques is not straightforward. Still, as in this study all catalysts featured the same support, this fraction is expected to be constant.

Before catalytic evaluation, the extrudates were crushed and sieved into a granulometry of 200 to 500 µm to prevent mass transfer limitations. As all elements were well distributed throughout the extrudates (Table 2), the metal to acid sites molar ratio in the tested powder particles was hence equivalent to the overall metal to acid sites ratio. Concerning the metal to acid sites distance, as the minimal powder particles size was at least one order of magnitude larger than the maximal Pt-acid site distance (200 µm vs. 10 µm), the latter is expected to be conserved in tested powder particles. The key difference, at the catalytic evaluation conditions, arising from the distinct metal location was then the metal-acid sites distance.

According to literature reports for hydroisomerization of *n*-paraffins [18, 27], a distance shorter than a few micrometers is required to ensure that diffusion of olefinic intermediates is not rate-limiting, pointing to an adequate intimacy between catalytic functions at the scale of zeolite crystals (0.5 µm max.). Conversely, this means that at the scale of the clusters (10 µm max.) the diffusion of olefinic intermediates might become relevant.

Impact of the metal-acid intimacy on hydroisomerization

At this point, it is of interest to compare not only the shaped catalysts, but also non-shaped ones (i.e. catalysts in which Pt is directly supported on the zeolite), as these are the most commonly studied in literature and are typically assumed to have the highest intimacy. According to our previous study on the role of metal-acid balance in Pt/HUSY catalyst, Pt loadings of 0.40 % and 0.70 % yielding dispersions of ca. 50 % are sufficient to balance the zeolite HUSY employed in this work [8b]. For each series, i.e. Pt/HUSY, Pt/HUSY+Al_2O_3, and Pt/Al_2O_3+HUSY, the catalysts with highest Pt loading, all considered to be well-balanced, are compared in Figure 8a). It is worth mentioning again that all catalysts were tested in powder form employing the same granulometry and at similar operating conditions.

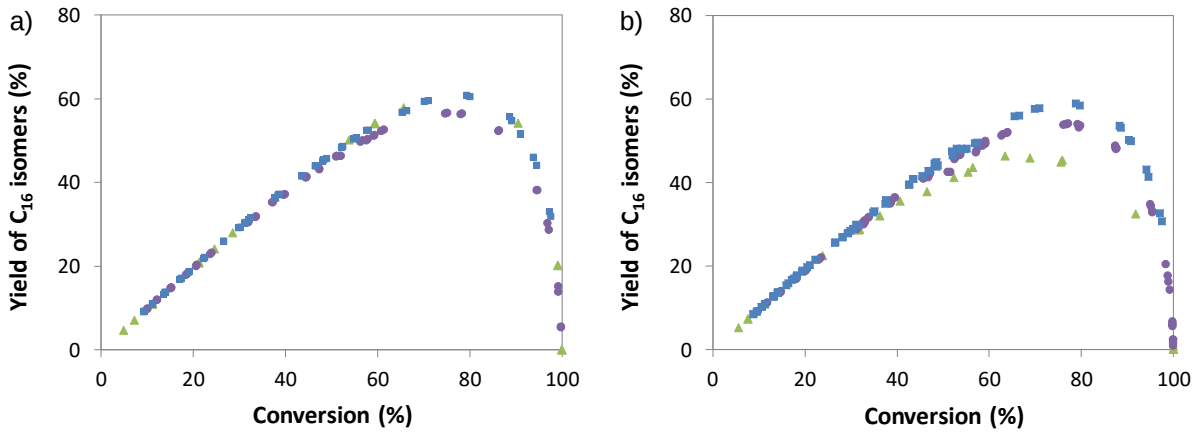

Figure 8: Yield of C_{16} isomers as function of conversion for a) well-balanced catalysts and b) poorly-balanced Pt/HUSY and balanced Pt-shaped catalysts. Catalysts: Pt/HUSY(▲), Pt/HUSY+Al_2O_3 (■), and Pt/Al_2O_3+HUSY (●). Pt loadings: a) 0.4%, 0.25%, 0.18%; b) 0.1%, 0.11%, 0.07%; respectively. Metal to acid sites ratio: a) 0.02, 0.071, 0.061; b) 0.003, 0.030, 0.024.

The yield of C_{16} isomers was markedly lower when Pt was deposed on the alumina than on the HUSY zeolite, irrespectively of the presence of a binder (Figure 8a). The shaping of HUSY zeolite has been already previously observed to be irrelevant for the hydroisomerization behaviour, provided that shaping is carefully controlled, platinum is located in the zeolite and homogeneously distributed throughout the extrudates [14a]. In this case, i.e. when deposing the HDH function in the zeolite, being the crystal size, and thus the maximal metal-acid sites distance, typically in the nanometer scale, the exact location of Pt (e.g. mainly inside the micropores as in HUSY or on the external surface of the crystals as in HBEA [22b]) shall not even truly matter for the hydroisomerisation performance.

Conversely, when platinum is located in the alumina, the Pt-acid site distance depends on the size of zeolite agglomerates, being thus much larger (100-10000 nm) than the expected Pt-acid distance when Pt is deposed in the zeolite. This decrease in isomerization selectivity can be hence attributed to the higher number of consecutive acid-catalysed steps occurring, due to the

longer Pt-acid sites distance. Such proposal can be qualitatively examined via a simplified reaction scheme based on isomerization followed by cracking [29]. For fixed operating conditions, the yield of feed isomers, and more particularly the maximum yield, depends on the ratio of the apparent kinetic constants for isomerization (k_I) and cracking (k_C) [30]. The higher the k_I/k_C ratio, the lower the fastest the consumption of C_{16} isomers as compared to their formation and, thus, the lower the C_{16} isomers yield. As the turnover frequency depends on k_I and was comparable, one may infer that k_C was greater over Pt/Al_2O_3+HUSY than over $Pt/HUSY+Al_2O_3$ catalysts. Therefore, the higher Pt-acid sites distance seems to have resulted in a higher apparent cracking constant which is in agreement with higher number of acid-catalysed steps encountered by the olefinic intermediates.

Scheme 1

These findings point to the detrimental role of long metal to acid sites distance, in agreement with most of the literature findings (mainly on HUSY but also on HBEA zeolite). Whenever the HDH function is located in the binder, the size of zeolite clusters determining the maximal Pt-acid sites distance, one possibility is to optimize the shaping conditions to prevent the formation of such (large) zeolite clusters. Concerning the potential positive role of longer metal-acid sites distances claimed in literature [20a], although this would provide interesting alternatives to design bifunctional catalysts [11, 20c], our study found no trace of such phenomenon. The observed increases in feed isomers yield when deposing the HDH function on alumina have been attributed to a predominant role of the external surface and pore mouths of the zeolite [20a, 20c]. However, in such case, a clear drop in catalytic activity, which was not observed, would be expected. Firstly, because only a small amount of the Brønsted acid sites of HUSY zeolites are on the external surface of the crystals (e.g. 11%, for the sample in this study [22b]). Secondly, because the confinement inside the zeolite structure is, at least partially, responsible for the high acidity of this class of materials. Whereas pore mouth sites have been suggested to be as acidic as the ones in the microporosity, the turnover frequency on the external surface sites can be expected to be significantly lower as compared to the inner ones, located in pores and cages.

Finally, it shall be noted that only by decoupling the effect of both the metal to acid sites molar ratio and intimacy (via well-balanced catalysts), the change in catalytic performance upon variation of the metal location could be herein confidently attributed to the metal to acid sites distance.

Interplay of metal-acid intimacy and balance in hydroisomerization

In addition to impacting the maximum C_{16} isomers yield of well-balanced catalysts (as just discussed), the intimacy might also impact the metal-acid sites ratio required to balance both functions. The epsilon value of the dual-function kinetic model is a descriptor of the metal-acid site molar ratio required to reach proper balance between the two functions [8b]. The higher is the epsilon value, the higher is the required metal-acid site molar ratio. The epsilon value of the dual-function kinetic model was similar for Pt/HUSY+Al_2O_3 and Pt/Al_2O_3+HUSY catalysts (Table S2). This suggests that the n_{Pt}/n_{Al} molar ratios required to reach plateau of maximum C_{16} isomers yield would be analogous for both shaped catalyst series (as can also be seen in the model lines in Figure 5). However, no experimental data at low n_{Pt}/n_{Al} was obtained for the Pt/HUSY+Al_2O_3 system so the epsilon value obtained with the model must be considered cautiously (Figure 5). In literature, as the distances between both functions became longer, the Pt-acid sites ratio required to reach a constant number of acid-catalysed steps was observed to diminish [16b]. According to the bifunctional mechanism, the lower requirement in terms of n_{Pt}/n_{Al} when diffusional limitations take place can be explained by the lower flow of olefinic intermediates between the two catalytic functions.

The interplay between metal-acid balance and intimacy can be evidenced when the catalysts featuring dissimilar metal-acid sites distance are compared at lower Pt loadings (Figure 8b). In such case, the maximum C_{16} isomers yield was much lower in Pt/HUSY whereas it remained similar for the shaped catalysts, as compared to the well-balanced catalysts (Figure 8a). In other words, Pt/HUSY became poorly-balanced whereas both Pt/HUSY+Al_2O_3 and Pt/Al_2O_3+HUSY were still well-balanced. Hence, catalysts with poor intimacy (Pt/Al_2O_3+HUSY) can outperform catalysts with optimal intimacy (Pt/HUSY) whenever proper balance between functions is not ensured in the latter.

The poor balance of Pt/HUSY in this case can be explained by the low metal-acid sites ratio (Figure 8b). In spite of the comparable Pt loadings, due to the dilution of the zeolite in the shaped support (16 wt.%) and the higher Pt dispersions in those catalysts, the metal-acid sites molar ratio is significantly lower in Pt/HUSY (0.003) than in the Pt shaped catalysts (0.024-0.030). Such assignment of the lower performance in Pt/HUSY to the metal to acid sites ratio was only possible because both metal to acid sites ratio and intimacy were quantified in all samples, particularly using techniques that probe the bulk of the catalysts (e.g. O_2-H_2 titration and EPMA) instead of providing a local qualitative picture which might not be representative of the whole sample (e.g. miscroscopic techniques).

In a nutshell, the results herein show that both balance and intimacy between metal and acid sites play a role in hydroisomerization, particularly when shaped, industrial-like, catalysts are at stake. Optimizing the catalyst performance requires hence the comprehensive study of both parameters.

Conclusion

The catalytic behaviour of bifunctional shaped HUSY zeolite catalysts was investigated for two distinct metal particle locations: either on alumina or on the zeolite. The platinum location was verified by a bulk technique confirming the selective metal deposition. The metal to acid sites molar ratio was varied in order to identify the well-balanced catalysts in both series, which were used for further comparison.

The turnover frequency per Brønsted site was observed to be equivalent regardless of Pt location. For Pt located on the zeolite, a superior plateau of maximal feed isomers yield was achieved as compared to when Pt was located on the alumina. Such difference was due to a lower selectivity towards multibranched feed isomers and so, most likely, to a higher number of consecutive acid-catalysed steps before hydrogenation when Pt was deposed on alumina as compared to a direct deposition on the zeolite. This result can be explained by the larger, micrometric Pt-acid sites distance when Pt was located on the alumina, due to large size of the HUSY zeolite clusters, as compared to the nanometric one when Pt was located on the zeolite. However, it has been shown that catalysts with poor intimacy (Pt/Al_2O_3+HUSY) can outperform catalysts with optimal intimacy (Pt/HUSY) whenever proper balance between functions is not ensured in the latter.

This work corroborates the requirement for sufficient metal-acid sites intimacy to achieve optimal performance whenever the metal-acid functions are well-balanced. Maximal catalyst performances are only reached if both metal-acid sites proximity and balance are suitable. As this depends on the reaction, operating conditions, metal and zeolite, the comprehensive study of proximity and balance between catalytic functions is crucial to the rational design of efficient bifunctional catalysts.

Experimental Section

Catalysts preparation

A commercial HUSY zeolite (CBV720) from *Zeolyst*, with a sodium to aluminium molar framework ratio of 0.01, was employed without any further treatment. The shaped zeolite was prepared by a mulling-extrusion method, described in detail elsewhere [14a], employing a commercial boehmite (Pural SB-3) from *Sasol* as a binder. Briefly, the zeolite, boehmite and *Methocel* powders were kneaded into a paste which was extruded through trilobal die resulting in a 1.6 mm diameter. Extrudates were then dried at 353 K overnight and calcined at 873 K over 2 h (heating rate of 5 K min^{-1}) under dry air (1.5 NL h^{-1} $g_{support}^{-1}$). The extrudates length was between 3 and 6 mm.

Aiming at a selective deposition of Pt in the zeolite crystals, excess impregnation of the extrudates with an aqueous solution containing $[Pt(NH_3)_4Cl_2]\cdot H_2O$ and NH_4NO_3 was performed [26a]. The amount of platinum deposited on the extrudates was modified by changing the concentration of Pt precursor in the solution. The $NH_4NO_3/Pt(NH_3)_4Cl_2$ molar ratio in the impregnation solution was equal to 120. The aqueous solution was added to the extrudates (8 mL per gram of extrudates) and the suspension was gently stirred for 24 h at room temperature. Afterwards the extrudates were rinsed with twice volume of distilled water. The impregnated materials were dried overnight at 383 K and then calcined in an air flow of 4 L h^{-1} g^{-1}. Three plateaux at 423, 523 and 623 K over 1 h each and a final plateau at 773 K over 2 h were performed. A heating rate of 5 K min^{-1} was used. This catalyst series are herein referred as "Pt/HUSY+Al_2O_3"

Aiming at a selective deposition of Pt in the alumina, ionic exchange with competition was performed [26d]. The procedure comprised a first step of ionic exchange with HCl followed by a second ionic exchange with H_2PtCl_6. As in the previous case, the amount of platinum deposited on the extrudates was modified by changing the concentration of Pt precursor in the solution. The dry extrudates were firstly humidified (using roughly twice the saturation volume of the support) and then mixed with an aqueous solution (4 mL per gram of dry support) containing 1.3 wt.% of hydrochloric acid. The suspension was stirred during 1 h and then decanted. The acidified extrudates were mixed with an aqueous solution (4 mL of solution per 1 g of dry support) containing H_2PtCl_6 during 24 h and then rinsed with twice volume of distilled water. Afterwards, the samples underwent the same thermal treatments as the Pt/HUSY+Al_2O_3 ones. This catalyst series are herein referred as "Pt/Al_2O_3+HUSY".

Materials characterization

Quantitative elemental analysis was performed by x-ray fluorescence. Samples were grinded and sieved into a granulometry under 200 µm. Measurements were carried out in a *Thermofischer Scientific Advant-X* instrument.

Platinum dispersion was determined by oxygen titration of chemisorbed hydrogen (O_2-H_2) in a homemade flow apparatus with a thermal conductivity detector. The pre-reduced saturated samples were pre-treated under H_2. Two cycles of hydrogen titration of chemisorbed oxygen and oxygen titration of chemisorbed hydrogen were consecutively performed at room temperature. The results presented correspond to the

average O_2 consumption in the two cycles; relative deviation between measures was inferior to 10%. The metal dispersion was calculated by means of a 0.75 O_2:Pt stoichiometric coefficient [30].

The electron probe micro analysis (EPMA) were carried out in a *JEOL JXA 8100* equipment. The extrudates were embedded in an Specifix-40 epoxy resin (*Struers, Ballerup*) that was prepolymerized to prevent carbon contamination [32] and polished to obtain a flat section. A thin conductive carbon layer was deposited to prevent surface charging effects. Samples were analysed using a 20 keV and 100 nA electron beam. Al was analysed on the Kα (2) line, Si on the Kα line, Pt on the Mα line, O was calculated based on the molecular formula of the following oxides: Al_2O_3 and SiO_2. For each sample, five profiles were measured on five different catalyst extrudates along a 3-fold symmetry axis of the extrudates (from a hollow to the lobe), further called the diameter of the extrudate. For every profile, 25 points were measured resulting in a constant step of about 56 µm. Local measured concentrations were then processed using the method of the distance transform [33] to obtain the overall concentration of each element in the extrudate.

In order to condense the elemental profiles into a single parameter, a distribution coefficient can be used. The distribution coefficient R_{element} is the ratio of the mean concentration along the extrudate to the overall concentration assuming a spherical grain of diameter $2r$ equal to the length of the profile [34] (Eq. 1). A distribution coefficient close to 1 means a uniform distribution of the element along the extrudate diameter. Otherwise, the coefficient will be higher than 1, if the concentration is greater in the core than at the edges (so-called egg-yolk distribution); and lower than 1 if the concentration is greater at the edges than in the core (so-called egg-shell distribution) [34].

To calculate the concentration of Pt in alumina and zeolite phases, the following procedure was applied [35]: for every analysis point, the local concentration in Al_2O_3 ($c_{Al_2O_3}$) and the local concentration in SiO_2 (c_{SiO_2}) were determined. Knowing the weight ratio $y = c_{SiO_2}/c_{Al_2O_3} = 20.4$ of the zeolite, the local concentration of alumina phase $c_{\text{alumina}} = c_{Al_2O_3} - y^{-1}c_{SiO_2}$, and of zeolite phase $c_{\text{zeolite}} = c_{SiO_2}(1 + y^{-1})$ was calculated for every point. The corresponding zeolite local weight fraction in the support (x_{zeolite}) was then calculated using Eq. 2.

$$R_{element} = \frac{r^2 \int_{-r}^{r} C_{element}(x)dx}{3\int_{-r}^{r} C_{element}(x)x^2dx} \qquad \text{Equation 1}$$

$$x_{\text{zeolite}} = \frac{c_{SiO_2}(1 + y^{-1})}{c_{SiO_2} + c_{Al_2O_3}} \qquad \text{Equation 2}$$

The plot of c_{Pt}, the local concentration of Pt, as function of x_{zeolite} was fitted to a straight line. Extrapolation of the line for $x_{\text{zeolite}} = 0$ and for $x_{\text{zeolite}} = 1$ gave the concentrations of Pt on the alumina phase and zeolite phase respectively.

Catalytic tests

The hydroisomerization of *n*-hexadecane was carried out in a high-throughput catalytic test unit with fixed-bed downflow reactors. The catalytic testing was fully automated, with the operating conditions of the catalytic bed of each reaction being monitored individually. To prevent any diffusional limitations, the catalysts were crushed and sieved into a smaller granulometry (0.2-0.5 mm). The catalyst was then pre-

treated using a hydrogen flowrate of 4 NL/h/g and heated at 5 K/min to a final reduction temperature of 723 K for one hour. The tests were performed at 1.1 MPa total pressure, a H_2 to *n*-C_{16} molar ratio of 10. The weight hourly space velocity (WHSV) ranged between 0.25 and 2.1 $g_{n\text{-hexadecane}}\ g_{catalyst}^{-1}\ h^{-1}$ and the reaction temperature ranged from 483 to 498 K in order to modify the conversion level.

Products were analysed on-line by a GC-FID apparatus equipped with low polarity capillary columns from *Agilent* (DB-1 and CP-Sil-5-CB). Deactivation of all samples was negligible at the end of the catalytic tests. Catalytic performances were calculated by mass balance to the carbon atoms at the outlet. n-C_{16} conversion was calculated as the amount of carbon atoms of the products divided by total amount of carbon atoms. The yield of a given product was calculated as the amount of carbon atoms of that product divided by total amount of carbon atoms. Activity was calculated as the apparent kinetic constant for first-order consumption of *n*-hexadecane per catalyst mass per unit of time. The average turnover frequency per Brønsted sites was defined as the activity per mole of Brønsted acid site of the zeolite (see Table 1).

Acknowledgements

The authors would like to thank C. Leroux for the work on the catalyst synthesis; M. Moscovici-Mirande, V. Delattre and C. James for the work on n-C_{16} hydroisomerization; V. Lefebvre, Y. Blouet, F. Fillali and A.-S. Gay for the work on electron microprobe; and N. Girod for the work on H_2-O_2 titration. Centro de Química Estrutural acknowledges the financial support of *Fundação para a Ciência e Tecnologia* (Project UIDB/0100/2020) and PhD grant (SFRH/BD/87927/2012).

Keywords: HUSY zeolite; hydroisomerization; metal-acid intimacy; metal-acid balance; shaping.

References

[1] aA. Primo, H. Garcia, *Chem. Soc. Rev.* **2014**, *43*, 7548–7561; bE. T. C. Vogt, G. T. Whiting, A. Dutta Chowdhury, B. M. Weckhuysen, in *Advances in Catalysis, Vol. Volume 58* (Ed.: C. J. Friederike), Academic Press, **2015**, pp. 143–314.

[2] F. Bertoncini, A. Bonduelle-Skrzypczak, J. Francis, E. Guillon, in *Catalysis by Transition Metal Sulphides* (Eds.: H. Toulhoat, P. Raybaud), Ed. Technip, Paris, **2013**, pp. 609–677.

[3] D. N. Gerasimov, E. V. Kashin, I. V. Pigoleva, I. A. Maslov, V. V. Fadeev, S. V. Zaglyadova, *Energy & Fuels* **2019**, *33*, 3492-3503.

[4] J. Weitkamp, *Chemcatchem* **2012**, *4*, 292–306.

[5] aE. Furimsky, *Catalysis Today* **2013**, *217*, 13–56; bU. Neuling, M. Kaltschmitt, *Journal of Oil Palm Research* **2017**, *29*, 137-167; cA. Daudin, N. Dupassieux, T. Chapus, in *Catalysis by Transition Metal Sulphides* (Eds.: H. Toulhoat, P. Raybaud), Ed. Technip, Paris, **2013**, pp. 739–755.

[6] aC. Bouchy, G. Hastoy, E. Guillon, J. A. Martens, *Oil & Gas Science and Technology - Rev. IFP* **2009**, *64*, 91–112; bG. Liu, B. Yan, G. Chen, *Renewable & Sustainable Energy Reviews* **2013**, *25*, 59–70; cE. F. Sousa-Aguiar, F. B. Noronhac, J. Faro, Arnaldo, *Catalysis Science & Technology* **2011**, *1*, 698–713.

[7] aK. Ragaert, L. Delva, K. Van Geem, *Waste Management* **2017**, *69*, 24-58; bD. Munir, M. F. Irfan, M. R. Usman, *Renewable and Sustainable Energy Reviews* **2018**, *90*, 490-515.

[8] aW. Wang, C. J. Liu, W. Wu, *Catalysis Science & Technology* **2019**, *9*, 4162-4187; bP. S. F. Mendes, J. M. Silva, M. F. Ribeiro, P. Duchêne, A. Daudin, C. Bouchy, *AIChE Journal* **2017**, *63*, 2864-2875; cV. M. Akhmedov, S. H. Al-Khowaiter, *Catalysis Reviews-Science and Engineering* **2007**, *49*, 33–139; dP. Maki-Arvela, T. A. K. Khel, M. Azkaar, S. Engblom, D. Y. Murzin, *Catalysts* **2018**, *8*, 27; eF. M. Mota, C. Bouchy, E. Guillon, A. Fecant, N. Bats, J. A. Martens, *Journal of Catalysis* **2013**, *301*, 20–29; fP. S. F. Mendes, J. M. Silva, M. F. Ribeiro, A. Daudin, C. Bouchy, *Catalysis Today* **2019**.

[9] R. L. Bedard, in *Zeolites in Industrial Separation and Catalysis* (Ed.: S. Kulprathipanja), Wiley-VCH Verlag GmbH & Co. KGaA, Weinheim, Germany, **2010**, pp. 61–83.

[10] S. Mitchell, N.-L. Michels, J. Perez-Ramirez, *Chemical Society Reviews* **2013**, *42*, 6094-6112.

[11] D. Y. Murzin, *Catalysis Letters* **2017**, *147*, 613-621.

[12] aA. Martin, H. Berndt, *Reaction Kinetics & Catalysis Letters* **1994**, *52*, 405–411; bA. Martin, H. Berndt, U. Lohse, U. Wolf, *J. Chem. Soc., Faraday Trans.* **1993**, *89*, 1277–1282; cN.-L. Michels, S. Mitchell, J. Pérez-Ramírez, *Acs Catalysis* **2014**, *4*, 2409–2417; dA. d. Lucas, J. L. Valverde, P. Sanchez, F. Dorado, M. J. Ramos, *Applied Catalysis a-General* **2005**, *282*, 15–24.

[13] aK.-Y. Lee, H.-K. Lee, S.-K. Ihm, *Top. Catal.* **2010**, *53*, 247–253; bK. Ito, H. Jang, K. Sakashita, S. Asaoka, *Pure and Applied Chemistry* **2008**, *80*; cX. Du, X. Kong, L. Chen, *Catalysis Communications* **2014**, *45*, 109–113; dL. Lakiss, J.-P. Gilson, V. Valtchev, S. Mintova, A. Vicente, A. Vimont, R. Bedard, S. Abdo, J. Bricker, *Microporous and Mesoporous Materials* **2020**, 110114.

[14] aP. S. F. Mendes, J. M. Silva, M. F. Ribeiro, A. Daudin, C. Bouchy, *Journal of Industrial and Engineering Chemistry* **2018**, *62*, 72-83; bL. Gueudré, M. Milina, S. Mitchell, J. Pérez-Ramírez, *Advanced Functional Materials* **2014**, *24*, 209–219.

[15] H. L. Coonradt, W. E. Garwood, *Industrial & Engineering Chemistry Process Design and Development* **1964**, *3*, p. 38.

[16] aF. Alvarez, F. R. Ribeiro, G. Perot, C. Thomazeau, M. Guisnet, *Journal of Catalysis* **1996**, *162*, 179–189; bN. Batalha, L. Pinard, C. Bouchy, E. Guillon, M. Guisnet, *Journal of Catalysis* **2013**, *307*, 122–131; cG. E. Giannetto, G. R. Perot, M. R. Guisnet, *Ind. Eng. Chem. Prod. Res. Dev.* **1986**, *25*, 481–490.

[17] F. Alvarez, F. R. Ribeiro, G. Perot, C. Thomazeau, M. Guisnet, *Journal of Catalysis* **1996**, *162*, 179-189.

[18] aP. B. Weisz, in *Advances in Catalysis, Vol. Volume 13* (Eds.: P. W. S. P. B. W. A. A. B. J. H. D. B. P. J. D. P. H. E. J. H. W. D.D. Eley, H. S. Taylor), Academic Press, **1962**, pp. 137–190; bN. Batalha, L. Pinard, Y. Pouilloux, M. Guisnet, *Catalysis Letters* **2013**, *143*, 587–591.

[19] aE. Gutierrez-Acebo, C. Leroux, C. Chizallet, Y. Schuurman, C. Bouchy, *ACS Catal.* **2018**, *8*, 6035-6046; bY. Zhang, D. Liu, Z. Men, K. Huang, Y. Lv, M. Li, B. Lou, *Fuel* **2019**, *236*, 428-436; cN. Batalha, S. Morisset, L. Pinard, I. Maupin, J. L. Lemberton, F. Lemos, Y. Pouilloux, *Microporous and Mesoporous Materials* **2013**, *166*, 161–166.

[20] aJ. Zecevic, G. Vanbutsele, K. P. de Jong, J. A. Martens, *Nature* **2015**, *528*, 245–248; bO. Ben Moussa, L. Tinat, X. J. Jin, W. Baaziz, O. Durupthy, C. Sayag, J. Blanchard, *ACS Catal.* **2018**, *8*, 6071-6078; cR. Glaser, *Nature* **2015**, *528*, 197–198; dK. Cheng, L. I. van der Wal, H. Yoshida, J. Oenema, J. Harmel, Z. Zhang, G. Sunley, J. Zečević, K. P. de Jong, *Angewandte Chemie* **2020**, *132*, 3620-3628.

[21] Z. Vajglová, N. Kumar, M. Peurla, L. Hupa, K. Semikin, D. A. Sladkovskiy, D. Y. Murzin, *Industrial & Engineering Chemistry Research* **2019**, *58*, 10875-10885.

[22] aP. S. F. Mendes, G. Lapisardi, C. Bouchy, M. Rivallan, J. M. Silva, M. F. Ribeiro, *Applied Catalysis A: General* **2015**, *504*, 17-28; bP. S. F. Mendes, F. M. Mota, J. M. Silva, M. F. Ribeiro, A. Daudin, C. Bouchy, *Catalysis Science & Technology* **2017**, *7*, 1095-1107.

[23] M. Kosmulski, *Journal of Colloid and Interface Science* **2011**, *353*, 1–15.

[24] aF. Ribeiro, C. Marcilly, *Revue de l'Institut Français du Pétrole* **1979**, *34*, 405–428; bJ. E. Samad, S. Hashim, S. Ma, J. R. Regalbuto, *Journal of Colloid and Interface Science* **2014**, *436*, 204–210; cF. Ribeiro, C. Marcilly, M. Guisnet, *Journal of Catalysis* **1982**, *78*, 267–274; dW. A. Spieker, J. R. Regalbuto, *Chemical Engineering Science* **2001**, *56*, 3491–3504.

[25] aM. J. Girgis, Y. P. Tsao, *Industrial & Engineering Chemistry Research* **1996**, *35*, 386–396; bV. Calemma, S. Peratello, C. Perego, *Applied Catalysis a-General* **2000**, *190*, 207–218.

[26] P. S. F. Mendes, J. M. Silva, M. F. Ribeiro, C. Bouchy, A. Daudin, *Journal of Industrial and Engineering Chemistry* **2018**.

[27] J. E. Samad, J. Blanchard, C. Sayag, C. Louis, J. R. Regalbuto, *Journal of Catalysis* **2016**, *342*, 203-212.

[28] P. S. F. Mendes, C. Chizallet, J. Pérez-Pellitero, P. Raybaud, J. M. Silva, M. F. Ribeiro, A. Daudin, C. Bouchy, *Catalysis Science & Technology* **2019**, *9*, 5368-5382.

[29] O. Levenspiel, *Chemical Reaction Engineering*, 3rd edition ed., John Wiley & Sons, Ltd, New York, **1999**.

[30] aC. H. Bartholemew, in *Catalysis: Volume 11, Vol. 11* (Eds.: J. J. Spivey, S. K. Agarwal), The Royal Society of Chemistry, **1994**, pp. 93–126; bJ. Prasad, K. R. Murthy, P. G. Menon, *Journal of Catalysis* **1978**, *52*, 515–520.

[31] L. Sorbier, E. Rosenberg, C. Merlet, *Microscopy and Microanalysis* **2004**, *10*, 745–752.

[32] L. Sorbier, F. Bazer-Bachi, Y. Blouet, M. Moreaud, V. Moizan-Basle, *Microscopy and Microanalysis* **2016**, *22*, 422–431.

[33] L. Sorbier, in *Catalysis by Transition Metal Sulphides* (Eds.: H. Toulhoat, P. Raybaud), Ed. Technip, Paris, **2013**, pp. 407–411.

[34] S. Kasztelan, N. Marchal-George, T. Cseri*, Vol. A1*, **2001**.

Table of Contents

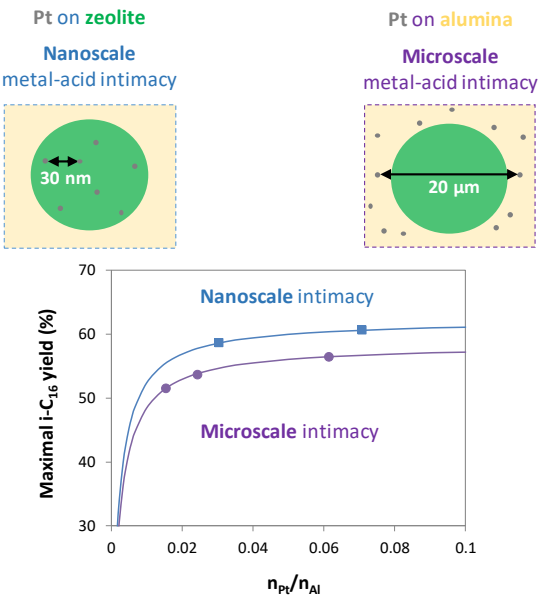

Design of efficient hydroisomerization catalysts is crucial to the sustainable production of liquid fuels, but the bifunctional character of the catalyst introduces additional complexity. To unravel this complexity, the interplay between the intimacy and balance of metal-acid sites was investigated over industrially-relevant shaped catalysts.